JOURNAL OF THERMOPHYSICS AND HEAT TRANSFER
Vol. 13, No. 4, October–December 1999

Impingement Heat Transfer on a Target Plate with Film Cooling Holes

Srinath V. Ekkad*
Louisiana State University, Baton Rouge, Louisiana 70803
and
Yizhe Huang† and Je-Chin Han‡
Texas A&M University, College Station, Texas 77843

Detailed heat-transfer distributions are presented for an array of jets impinging on a target plate with a staggered array of film cooling holes. The flow impinges on the target plate through a row of impingement holes and exits the channel from the sides and through the film holes. The top plate has 12 rows of impingement holes, and the target plate has 11 rows of film holes. The impingement holes and the film holes have the same diameter and are staggered such that the air from the impingement hole does not exit directly through the film hole. The setup is typical of an impingement/transpiration cooled gas turbine airfoil. Additional to the flow exiting through the film holes, there is an exit for crossflow after impingement. The exit opening of the impingement channel is changed to provide three different spent air exit directions. The detailed heat-transfer coefficient distributions were measured using a transient liquid crystal technique. Results are presented for a range of jet Reynolds numbers between 0.4×10^3 and 2.0×10^4 with different exit flow orientations. Heat-transfer results for the target plate with film holes are compared with those without film holes under the same flow conditions. Film extraction reduces crossflow effects on jet impingement heat transfer. However, overall averaged heat-transfer rates on the target surface appear less affected by presence of film hole for cases where the crossflow is generated in only one direction.

Nomenclature

A = heat-transfer surface area
d = impingement jet hole diameter and coolant extraction hole diameter
H = distance between the impingement plate and the target plate
h = local convection heat-transfer coefficient, W/m^2-K
k = thermal conductivity of acrylic material
k_{air} = thermal conductivity of air
m_c = crossflow mass flow rate
m_f = film hole mass flow rate
m_j = impingement hole mass flow rate
Nu = Nusselt number, hd/k_{air}
Pr = Prandtl number
Re_j = average jet Reynolds number, $\rho V_j d/\mu$
s = jet-jet spacing
T_g = color change temperature of the liquid crystal (red–green)
T_i = initial temperature of test section
T_m = mainstream temperature of the flow
t = time of liquid crystal color change
V_j = average jet velocity
X = axial distance on the target surface
Y = spanwise distance on the target surface
α = thermal diffusivity of test section
μ = fluid dynamic viscosity
τ = time step

Received 14 September 1998; revision received 20 April 1999; accepted for publication 23 April 1999.

*Assistant Professor, Mechanical Engineering Department; ekkad@me.lsu.edu.
†Research Assistant, Department of Mechanical Engineering; currently Mechanical Engineer, Motorola, Inc., Austin, TX 78740.
‡HTRI Professor, Department of Mechanical Engineering; jchan@mengr.tamu.edu. Associate Fellow AIAA.

Introduction

HEAT-TRANSFER enhancement using jet impingement is a commonly applied technique for several convective applications such as heat treatment of metals, paper drying, electronic component cooling, and turbine component cooling. With increased turbine inlet temperatures heat-transfer enhancement to remove heat from the airfoil external surface has gained importance. Jet impingement has been used as a heat-transfer augmentation method inside gas turbine airfoils for several decades. A combination of jet impingement with transpiration film cooling has been identified as a possible highly effective cooling system. The results from this study can also be applied to any geometry with double-wall cooling schemes where crossflow is an important effect. One such example is Rolls-Royce Allisons' Lamilloy cooling pattern.

Experimental studies of impingement surface heat transfer for gas turbine applications were reported by Chupp et al.,[1] Kercher and Tabakoff,[2] Florschuetz et al.,[3,4] and Behbahani and Goldstein.[5] Downs and James[6] summarized findings relating to parametric effects of geometry, temperature, interference and crossflow, turbulence levels, surface curvature, and non-uniformity of jet array on jet impingement heat and mass transfer. Obot and Trabold[7] show that heat transfer for an array of jets increases with decreasing jet-to-jet spacing. Viskanta[8] and Huber and Viskanta[9,10] pointed out many different factors that influence heat transfer in multiple jet impingement systems such as wall-jet interaction, separation distance, jet-jet spacing and diameter, crossflow or exit of spent air, the orifice arrangement in line or staggered and target surface condition.

Kercher and Tabakoff[2] and Florschuetz et al.[3,4] presented heat-transfer correlations for jet impingement with crossflow effects on surface without film extraction. They presented correlations for both in-line and staggered jet hole patterns, including effects of geometric patterns. Bunker and Metzger[11] measured local heat-transfer characteristics in large-scale models of turbine blade impingement-cooled leading-edge regions. Results indicated an increase in heat transfer with approximately a 0.6th power of jet Reynolds number. Increases in heat transfer were noted with decreasing leading-edge sharpness as well as with decreasing nozzle-to-apex distance. An increase in spanwise-average heat transfer was noted with decreasing jet pitch-to-diameter ratio. Van Treuren et al.[12] studied impingement heat

transfer under in-line and staggered arrays of jets using a transient liquid crystal technique. They measured both local heat-transfer coefficient and adiabatic wall temperature under the impingement jets; however, they studied the effect of crossflow in only one direction. Huang et al.[13] presented results for impinging orthogonal jets on a target surface without film holes and three exit-flow orientations. They confirmed that the heat-transfer distributions on the target surface are significantly affected by crossflow direction. Crossflow effects are minimal when the flow exits toward both directions after impingement. Results were correlated for all three exit directions with the jet Reynolds number as parameter. The present study uses the same test setup used by Huang et al.[13] However, the target surface is replaced with a new target surface with film holes. The results from Ref. 13 are compared to the results from the present study.

In the past there have been a few investigations on impingement heat transfer for a target surface with film extraction (so called impingement/effusion cooling, impingement/transpiration cooling, and impingement with removal through vent holes). In this study the internal surface heat transfer is affected by three parameters: the jet impingement through the jet orifices, the crossflow induced by jet impingement in the channel, and the flow through the film holes. Several works by Andrews et al.[14] have focused on the effect of impingement and/or effusion (transpiration) cooling on external surface heat transfer. The focus of the present study is the internal surface heat transfer.

A target surface with film holes allows for extraction or bleeding of a portion of the internal cooling flow to provide film cooling along the airfoil external surface. Film extraction has been investigated by Hollworth and Dagan[15] and Hollworth et al.[16] They presented averaged and local heat transfer for an impingement target surface that also had film extraction through orifices. The jet spacing varied from 5 to 20 jet diameters in square arrays and jet Reynolds number varied from 0.3×10^3 to 3.5×10^4 in their tests. The averaged heat-transfer results indicated that a staggered configuration of the jet holes and film extraction holes was better than the in-line configuration. Metzger and Bunker[17] investigated the local heat transfer in internal impingement cooled turbine airfoil leading-edge regions with film extraction. Results suggest that heat transfer primarily depends on jet Reynolds numbers with smaller influences from the flow extraction rate. They pointed out that with jet holes and bleed holes in line bleed flow leads to generally increased heat transfer, which is the exact opposite conclusion presented by Hollworth et al.[16] Hence, it is clear that the jet holes and film hole configuration depend on the location on the airfoil. On a flat surface staggered configuration provided higher heat transfer, and on an airfoil leading edge in-line configuration provided higher heat transfer. Recently, Gillespie et al.[18] studied the heat transfer inside cast impingement cooling configuration. The cooling application is for double-wall cooling applications where the air goes through jet holes impingement into a small cavity between the internal wall and the external wall. The coolant is then ejected on the external surface through film cooling holes. Their geometry does not have the array of jet and film holes as in the present study. Also, this geometry produces no crossflow effect.

The present study provides detailed heat-transfer distributions on an impingement target surface with film extraction. This study is a continuation to the study by Huang et al.[13] This is the first study to focus on impingement heat transfer to a target plate with film holes affected by different crossflow directions. The transient liquid crystal image method used in this study is the same as that presented by Huang et al.[13] Three spent air exit directions are employed to evaluate the crossflow effect on the detailed heat-transfer coefficient distributions of the target surface. Comparisons with the results from Huang et al.[13] can help understand the effects of film extraction on heat transfer levels over the target surface.

Test Description and Apparatus

Figure 1 shows the schematic of the test section. There is a plenum chamber (91.44 cm long) through which the flow develops before entering the test section. The test section consists of two channels joined by a jet plate, which has an array of jet holes with diameter d of 0.635 cm. The length of the test section is 30.48 cm. Top chamber is denoted the pressure channel, and the bottom chamber is denoted the impingement channel. The pressure channel has a cross-section area of 10.16×2.54 cm, and the impingement channel has a cross-section area of 10.16×1.905 cm. The jet-plate thickness is equal to the jet hole diameter such that the L/d ratio of the hole is 1.0, which is typical for effusion/transpiration cooling. There are 12 rows of 4 holes each, and a total of 48 holes on the jet plate. The jet-to-jet spacing s is four times the jet hole diameter in both X and Y directions. The distance between the jet plate and the impingement target surface H is three times the jet hole diameter. The film hole diameter d is 0.635 cm (same as jet hole diameter). The target impingement surface has 11 rows of 3 holes and a total of 33 holes on the target impingement surface. The jet holes and the film holes are staggered in location such that the air from the jet holes always impinges on the target plate midway between holes (without crossflow effects). The total area ratio of the all film holes to all jet holes is 33/48. The jet-plate and target-plate geometries are typical in airfoils cooled by a combination of jet impingement and transpiration cooling as shown in Fig. 1. The entire test section is made of acrylic material to minimize conduction losses during the transient test. The impingement target surface is painted black and sprayed with a thin coating of thermochromic liquid crystals.

The data acquisition system consists of a red–green–blue (RGB) camera, a PC with a frame grabber board, and commercial image processing software. The composite color signal is split into red, green, and blue colors and is passed on to the color frame grabber board in the PC. The frame grabber board is programmed to analyze the color change using the software package. The software analyzes the picture frame by frame for color changes. The analysis records the time of transition of the liquid crystals from colorless to start of green band at each point on the test surface (100×280 data points). A time-of-color change from colorless to appearance of green is measured at every pixel location on the test surface. More details are presented by Huang et al.[13]

Figure 2 shows the sketch of the channel with three exit flow orientations. The three exit flow orientations are obtained by changing

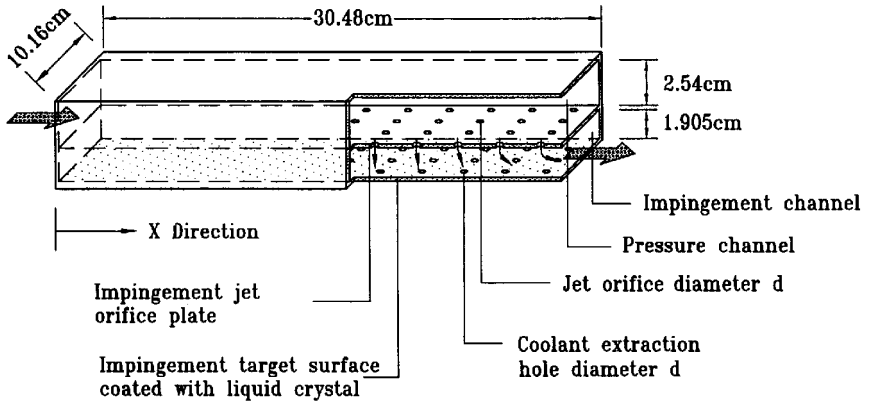

Fig. 1 Schematic of the test section.

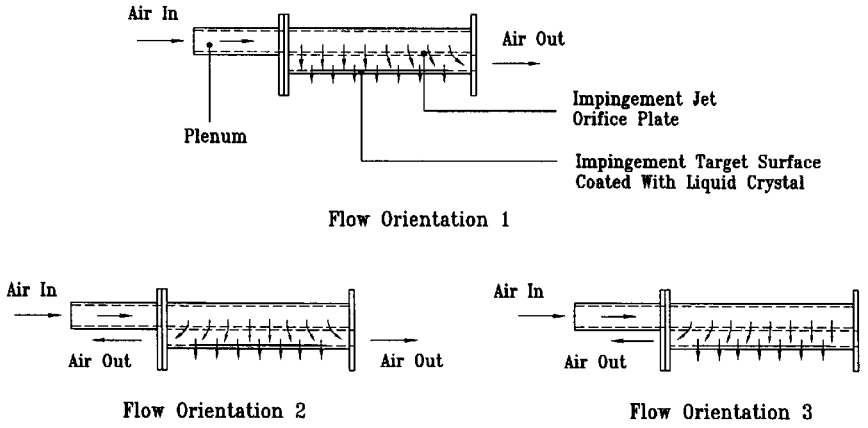

Fig. 2 Flow exit orientations.

the flow discharge openings. The three exit openings provide different local jet velocities and flow rates through the jet impingement holes and the film extraction holes. The inlet flow in the pressure channel and the exit flow in the impingement channel are coflowing (flow direction is same) for orientation 1, co- and counterflowing for orientation 2, and only counterflowing for orientation 3.

Theory

The local heat-transfer coefficient h can be calculated from the following equation by knowing the initial temperature ($T_i \sim 27°C$), mainstream temperature ($T_m \sim 50°C$), and by measuring the color change from time t for the liquid crystal coated surface to reach color change temperature ($T_g \sim 32.7°C$). The duration of the testing time is kept small so that a semi-infinite solid assumption is valid for a test plate of 0.508-cm thickness. The mainstream is heated to a temperature that produces color change times from 10–70 s. The testing time is much lower than the time required for the temperature to penetrate the acrylic wall. Because the test surface does not see a true step change in mainstream temperature, the solution must include the time history of the mainstream temperature:

$$T_g - T_i = \sum_{j=1}^{N} \left\{ 1 - \exp\left[\frac{h^2 \alpha (t - \tau_j)}{k^2} \right] \operatorname{erfc}\left[\frac{h\sqrt{\alpha (t - \tau_j)}}{k} \right] \right\} (\Delta T_{m_j})$$

A chart recorder measures the gradual change of the mainstream temperature at the entrance to the test section during the transient test. The time history of the mainstream temperature is reproduced as a series of step functions. $\Delta T_{m,j}$ and τ_j are the temperature and time-step changes from the chart recorder output. Huang et al.[13] present more details on the theory used to calculate the heat-transfer coefficients. The preceding equation is solved to obtain the local heat-transfer coefficient at every point on the measured region (there are totals of 280 points in the X direction and 100 points in the Y direction). The heat-transfer coefficient obtained from the preceding equation is based on the inlet temperature to the pressure channel.

Procedure

The test section connects to a compressor-based air supply with a standard orifice meter for measuring the flow rate. The mainstream flow rate is controlled and heated to a preset temperature using an in-line air heater. A test run begins with heated air diverted away from the test section so that the test channel walls remain at the laboratory ambient temperature. The valve remains in the diverted position until steady flow and a preset temperature have been achieved in the diversion flow loop. Then, the valve is suddenly switched to route the hot air into the pressure channel, expend through the jet orifice plate, and impinge on the target test surface. The data acquisition program and the chart recorder simultaneously switch on to measure color change time and mainstream temperature data, respectively. The data acquisition system records the transition time for the liquid crystal color change from colorless to green at every point on the test surface and transfers the data into a matrix of times of color change over the entire surface. A strip chart recorder measures the varying mainstream flow temperature T_m during the test. The heat-transfer coefficient is then calculated using the preceding equation at every point on the test surface.

The average uncertainty in heat-transfer coefficient measurement, estimated by the method of Kline and McClintock,[19] is about ±6.5%. The individual uncertainties in the measurement of the time of color change ($\Delta t = \pm 0.5$ s), the mainstream temperature ($\Delta T_m = \pm 1°C$), the color change temperature ($\Delta T_w = \pm 0.2°C$), and the wall material properties ($\Delta \alpha / k^2 = \pm 5\%$) are included in the calculation of the overall uncertainty in the measurement of h. The worst region for uncertainty is in the region where one-dimensional solid assumption may be violated. This region is around the edges of the film holes. The heat-transfer coefficients in these regions may be overpredicted by as much as 17%.

Results and Discussions

Flow Measurements

Local pressure distributions were measuring by placing static-pressure taps inside the test section for a target plate with film holes. Static pressures were measured inside the pressure channel and the impingement channel. Based on local pressure measurements, the local jet mass flow rates can be calculated. Also the difference in local pressure to ambient pressure in the impingement channel is used to obtain the exit crossflow rates. The impingement jet flow rate, film hole flow rate, and crossflow rate distributions along the channel are presented for an average jet Reynolds number of $Re_j = 9600$. The flow enters the pressure channel of the test section from one direction causing an uneven distribution of flow through each jet row for all three cases. The results are presented as a ratio of local mass flow with respect to the total mass flow through the test section.

Figure 3a presents the impingement jet flow rate distributions for all the three exit flow orientations. The jet mass flow rates are almost uniform across the channel for orientations 1 and 3, which may be because the flow enters the pressure channel with a strong axial velocity then enters the impingement channel through jet holes and exits in the only one direction. For orientation 2 in which case the flow exits both directions after impingement, the flow rates are higher through jet holes farther downstream. The cross velocity of the flow into the pressure channel may induce more flow to exit in the same direction as the entrance flow. However, the same does not happen for orientation 1. Compared to the flow data of Huang et al.,[13] flow orientation 1 appears to be significantly affected by the presence of film holes on the target surface. Flow orientations 2 and 3 appear less affected in the flow distributions through the holes.

Figure 3b presents the flow rates exiting through the film holes on the target surface. Flow orientation 1 shows an increase in exit flow rates from the first row to the sixth film hole row, and then the flow rates appear to stay constant. If you observe the direction of

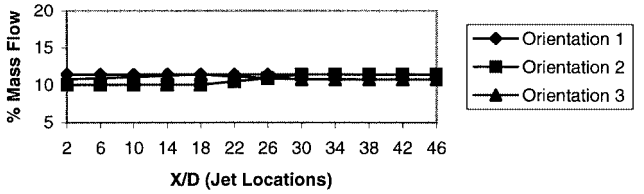

a) Impingement flow distributions

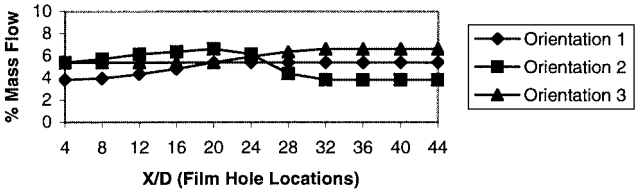

b) Film hole flow distributions

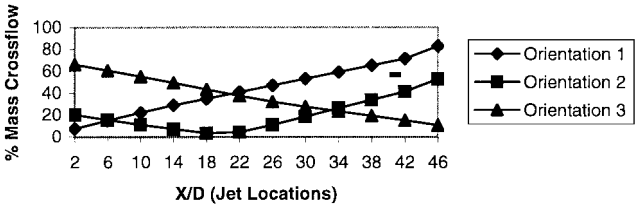

c) Crossflow distributions

Fig. 3 Jet flow rate, film flow rate, and crossflow rate distributions.

the crossflow, it appears consistent. For orientation 2 the flow rates increase from small X/D locations to about middle of the channel, the flow rates drop significantly in the middle rows, and then the distributions appear uniform through the holes at large X/D. For orientation 3 the flow rates are around 4% at low X/d for the first five film hole rows, then the exit flow rates increase a little for the rows at large X/D.

Figure 3c presents the ratio of the crossflow rate to total mass flow rate across the length of the channel. The crossflow develops from small X/d to exit for orientation 1. The crossflow is a minimum at the center of the channel for orientation 2 where the flow exits in both directions. The crossflow exits toward the low X/d direction for orientation 3. Compared to the flow data presented by Huang et al.,[13] the crossflow rates are much lower. The flow rate at the exit for orientation 1 is around 50% of total flow rate in this case compared to 100% for the case without film holes. That implies that about 50–60% of the flow that enters the impingement channel leaves through the film holes depending upon the crossflow orientation. The heat-transfer distributions and jet impingement are significantly influenced by the jet hole flow, film hole flow, and crossflow rate distributions. The effect of crossflow combined with loss of flow through film holes contributes to different heat-transfer levels compared to the study by Huang et al.,[13] where the jet impingement was dominated by crossflow effects.

Heat-Transfer Coefficient Measurements

Heat-transfer tests were performed at four average jet Reynolds numbers Re_j of 4850; 9550; 12,800; and 18,300 for all three flow orientations. Figures 4–6 present the detailed Nusselt number distributions for all three exit flow orientations at different jet Reynolds numbers. The two-dimensional surface plots show the Nusselt number variations on the target surface in the X/d (crossflow-axial) direction and in the Y/d (spanwise) direction. Results are presented from $X/d = 3.5$ to 44.5 along the axial direction X over the entire span of the target surface. The impingement and film hole locations are indicated for each flow orientation. The impingement hole locations are shown with upward arrows indicating inflow, and the film hole locations are shown as downward arrows indicating outflow. Nusselt numbers increase on the entire target surface with an increase in jet Reynolds number for all three flow orientations.

Figure 4 presents the detailed Nusselt number distributions for exit flow orientation 1. The inlet flow and exit flow are coflowing

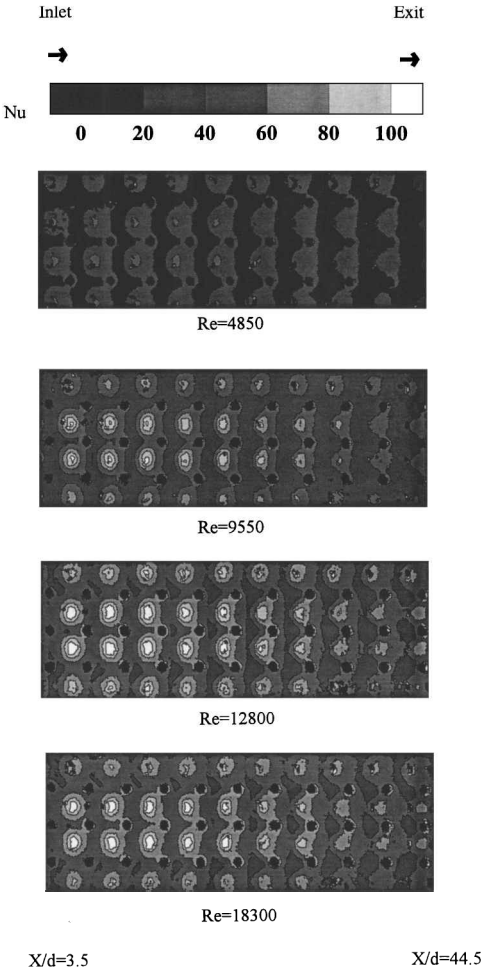

Fig. 4 Detailed Nusselt number distributions for flow orientation 1.

in this case. The jets impinge completely on the target surface at small X/d locations as no crossflow exists in that region. As the flow from the jets at small X/d develop a crossflow, the jets from the holes at large X/d are swept away from the test surface reducing impingement heat-transfer levels. Also the jet impingement location on the target surface is skewed depending on the crossflow strength. Compared to the cases in Huang et al.,[13] the presence of film holes causes the impinging air to also exit through the film holes after impingement. This reduces the crossflow levels compared to the target surface without film holes as shown in Fig. 3. The Nusselt numbers in the regions between the impinging jets are enhanced because of the flow migrating toward the film holes at higher velocity than the crossflow. Because of crossflow effect, the migration of the impinging air to the film hole is only from the upstream (direction of crossflow) jet holes. The presence of the film holes was expected to reduce crossflow effects and increase target surface heat-transfer coefficients. However, that does not seem to be the case as seen from the detailed distributions. The jet impingement from the jet holes at the outer edges of the channel (Y direction) is reduced because of edge effects producing lower Nusselt number values.

Figure 5 presents similar detailed Nusselt number distributions for flow exit orientation 2. In this case the exit crossflow is in both directions. The highest impingement Nusselt numbers are obtained in the region of $X/d \sim 14$–22, because of the minimum crossflow in that region, except for $Re_j = 4850$. The jet impingement Nusselt numbers appear higher for this case than orientation 1. The impinging air, unaffected by crossflow in the bulk of the impingement channel, exits freely out through the film holes causing significantly reduced impingement. The migration of impinging air is toward all the film holes around it in the middle of the channel. At small and large X/d locations, the direction of the migration is only to the holes decided by the direction of the crossflow. As in Huang et al.,[13] the bulk of the impinging jets for this case are unaffected

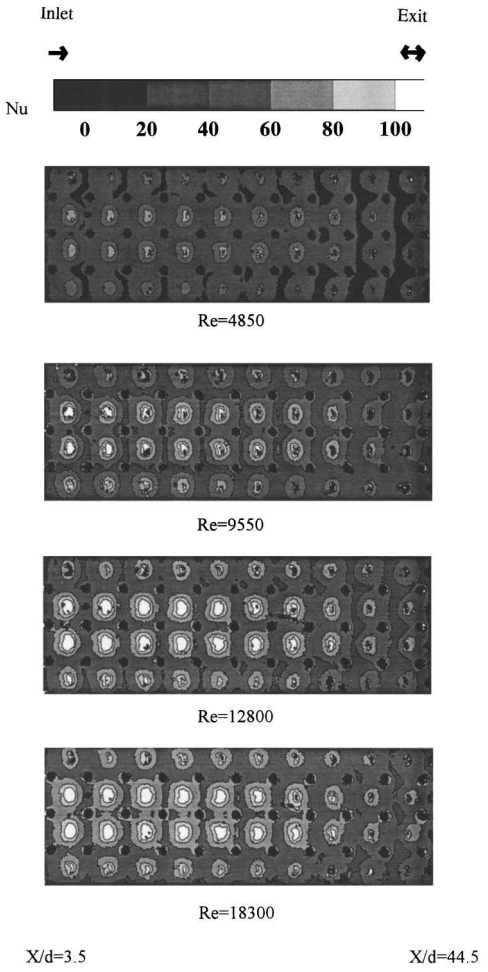

Fig. 5 Detailed Nusselt number distributions for flow orientation 2.

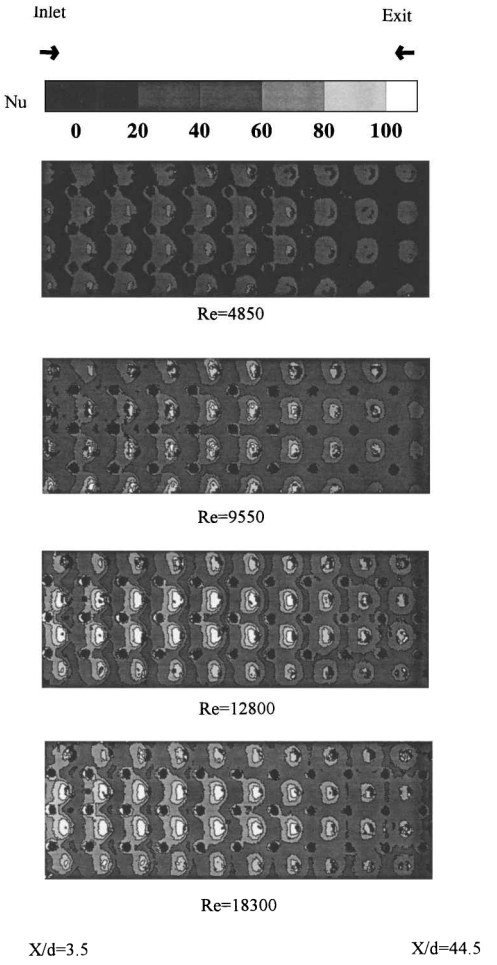

Fig. 6 Detailed Nusselt number distributions for flow orientation 3.

by the crossflow. The crossflow strength is smaller (Fig. 3) in both directions.

Figure 6 presents the detailed Nusselt number distributions for flow exit orientation 3. In this case the exit flow direction is counterflowing to the inlet flow. Because of this reason, the crossflow effect is stronger at the small X/d locations. The jet impingement would be expected to be strongest at large X/d because of small crossflow. However, it is not true. More coolant exits out of the impingement holes at small X/d because of large pressure difference and lesser resistance to flow. The effect of the crossflow is to push the jets away from the target surface as evidenced by the heat-transfer distributions. The coolant migration toward the film holes is in the direction of the induced crossflow in this case also because of the alteration of jet structures such that the impinging air is pushed in the direction of the crossflow and thus feeding only the two holes on the downstream side.

The shape of the jet impingement heat-transfer pattern for all three exit flow orientations is interesting. For orientation 1 the jet impingement heat-transfer pattern shows high heat transfer in the core of the jet but slightly shifted toward the large X/d direction (crossflow). For exit orientation 2 the jet appears to be impinging completely on the target surface because of reduced crossflow effects. For flow orientation 3 the jet impingement heat-transfer patterns appear reverse compared to the pattern for orientation 1. The direction of crossflow significantly affects the jet impingement heat-transfer pattern underneath the jet and also the direction of jet impingement flow migration toward the film holes. The jet impingement region appears to be wider and the local heat-transfer coefficients are comparatively lower than the data of Huang et al.[13] The presence of film holes between the jet holes makes the jet flows to migrate toward the film holes reducing jet impingement levels and spreading the jets over a larger surface area. This causes spreading of heat-transfer coefficients with a lower jet core heat-transfer coefficient. This is the main effect of the film extraction on heat-transfer coefficients. Also, the crossflow effect is reduced so the jets are not pushed away from the surface as strongly as in the case of Huang et al.[13] More uniform and higher heat-transfer coefficients caused by jet impingement produces similar overall heat-transfer levels as in the case of the target plate without film holes.

Figure 7 presents the effect of Reynolds number on spanwise-averaged Nusselt number distributions for all three flow orientations. The arrows indicate the jet hole location, and the black dots indicate the film hole locations. The Nusselt numbers at every crossflow streamwise location X, from the detailed distributions presented earlier are averaged over the entire span Y. The area averaging technique discounts the film hole area on the target surface. Nusselt numbers increase with increasing Reynolds number for all the three exit flow orientations. The highest Nusselt number underneath the jet occurs to the right of the jet hole location for orientation 1, directly underneath the jet hole location for orientation 2, and to the left of the jet hole location for orientation 3. This observation clearly indicates the crossflow effect for each case. Nusselt number decreases with increasing X/d for orientation 1. High Nusselt numbers beneath the jets appear to be similar for all three crossflow orientations. This is different than the pattern observed by Huang et al.,[13] who observed that flow orientation 2 produced much higher heat-transfer coefficients underneath the jet than the other two flow orientations. Determining the effect that the presence of film holes has on the target surface heat transfer from this plot is difficult.

Figure 8 presents the comparison of spanwise-averaged Nusselt number distributions for a target surface without film holes[13] to a target surface with film holes for $Re_j = 4850$. The comparison shows that for flow orientations 1 and 3 the spanwise-averaged Nusselt numbers are similar for the two target plates. However, there is a

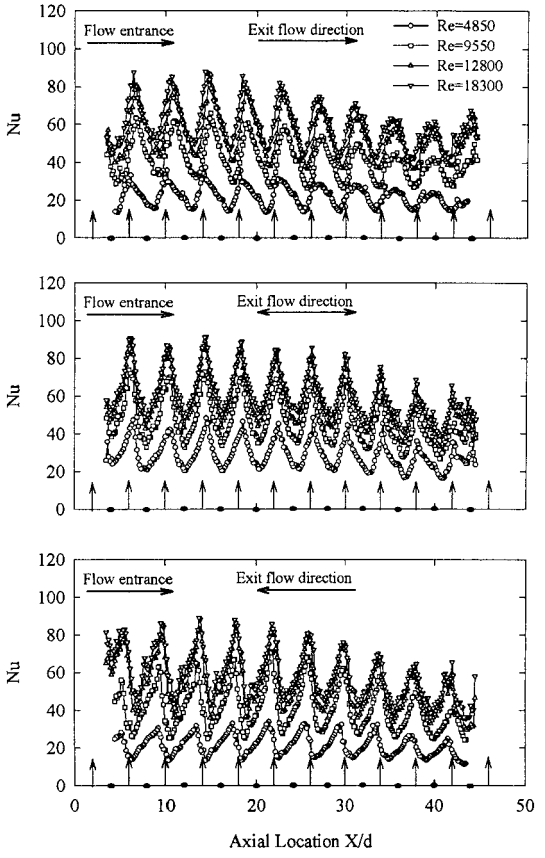

Fig. 7 Effect of Reynolds number on spanwise-averaged Nusselt number distributions.

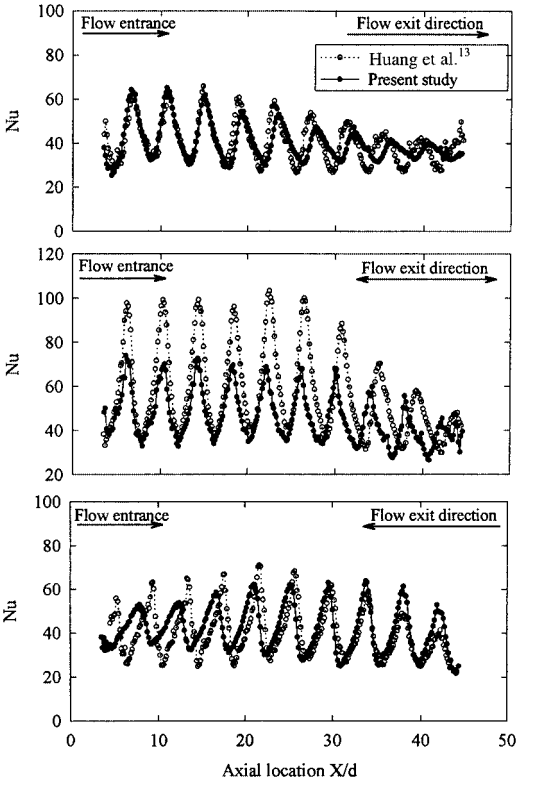

Fig. 8 Comparison of Nusselt number distributions on target plates with and without film holes for $Re = 9550$.

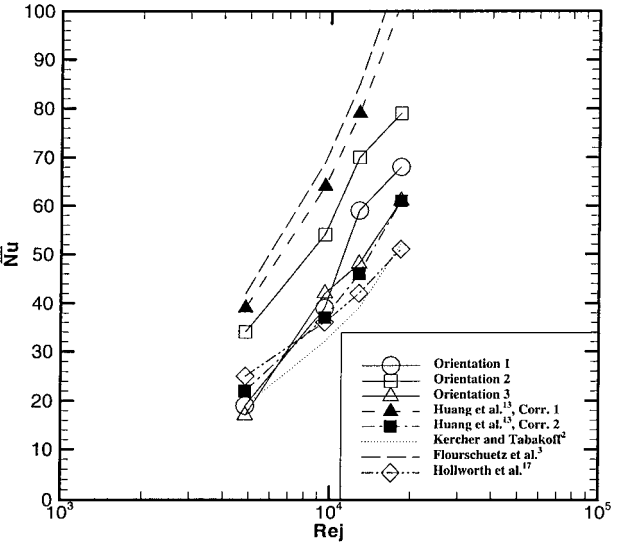

Fig. 9 Overall averaged Nusselt number comparisons with published correlations.

significant drop for orientation 2 from a target surface without holes to a target surface with holes. The increased jet impingement caused by reduced crossflow and spreading of jets because of flow migration in regions between impingement produces similar levels of Nusselt numbers for orientations 1 and 3. For flow orientation 2 the effect of coolant holes is to reduce jet impingement heat transfer because of the some flow migration toward the film hole before impingement. This reduces the heat-transfer coefficient directly underneath the jet but increases slightly the Nusselt numbers in the region between the jets. Because crossflow effect for this flow orientation was not an issue even when the target plate was without film holes,[13] film extraction is the main cause of the drop in heat-transfer levels for orientation 2. This comparison is expected to change because the Nusselt numbers are computed using local bulk fluid temperatures.

Figure 9 compares the overall averaged Nusselt number for each case and Reynolds number with existing published correlations[2,3,13] for target surface without film holes and corelation[17] for a target surface with film extraction. Kercher and Tabakoff[2] studied impingement on a target surface with strong crossflow effect similar to that in orientation 1. Based on all geometrical parameters, they proposed a correlation of the form $Nu = \phi_1\phi_2 Re^m (Z/d)^{0.091} Pr^{1/3}$, where Φ_1 and Φ_2 are constants based on X/d and Y/d. Florschuetz et al.[3] proposed a correlation for jet impingement for minimum crossflow given as $Nu = 0.363(X/d)^{-0.554}(Y/d)^{-0.422}(Z/d)^{0.068} Re_j^{0.727} Pr^{1/3}$. The correlations from Huang et al.[13] are also included. The correlation for orientation 2 from Huang et al.'s[13] study is given as $Nu = 0.082 Re^{0.727}$ (corr. 1). The correlation for orientations 1 and 3 is given as $Nu = 0.035 Re^{0.76}$ (corr. 2). Also shown is the relation between Nusselt number and jet Reynolds number from the study by Hollworth et al.[17] The data from this study is plotted as a line though Hollworth et al.[17] did not provide any correlation for their data.

Comparing the various correlations to the data from this study, the Nusselt number variation with jet Reynolds number for orientations 1 and 3 do not deviate much from Huang et al.'s[13] correlation 2. This was quite evident from the span-averaged data plot in Fig. 8. However, there is a significant drop in Nusselt numbers comparing Huang et al.'s[13] correlation 1 with the data for orientation 2, which is also well explained in Fig. 8. Kercher and Tabakoff's correlation is lower than the data for orientations 1 and 3 because of the strong crossflow effect in their study. Florschuetz et al.[3,4] show much higher Nusselt numbers for their pure impingement correlation with minimum crossflow. Finally, Hollworth et al.[17] correlation matches well with the data for orientations 1 and 3.

Conclusions

The effect of exit flow orientation on heat transfer to a target surface with film holes for multiple jet impingement arrays has been

investigated. The results are compared to the results for a target surface without film holes.[13] This is the first study to focus on heat transfer to a target plate with film holes affected by crossflow direction. The conclusions are the following:

1) Different exit flow orientations produce different heat-transfer distributions on the target plate. Results show that flow orientation 2 produces the highest Nusselt numbers compared to orientations 1 and 3 because the crossflow effects are smaller for orientation 2 compared to that for the other two orientations.

2) For flow orientations 1 and 3 Nusselt number distributions are not significantly affected by the presence of film holes on the target surface. However, for orientation 2 there is a 20% reduction in Nusselt numbers for a target surface with film holes because of the migration of impinging air toward the film holes and thus reducing strong impingement effect. The direction and strength of the crossflow also dictates the direction of flow migration toward film holes on the target surface.

3) The highest Nusselt number for flow orientation 1 occurs to the right side of the jet hole location, underneath the jet location for orientation 2, and to the left side of jet location for orientation 3. Crossflow direction and strength depending on axial location along the channel affect jet impingement heat transfer significantly.

4) Although the heat-transfer coefficient is only slightly affected for orientations 1 and 3 and significantly (20%) for orientation 2, the benefit of additional cooling in the form of film cooling on the outer surface is extremely valuable. The coolant exiting the target plate forms a film on the outer surface and reduces heat flux into the target plate from the hot side. This additional cooling greatly improves cooling for components such as turbine blades operating in high-temperature environments.

Acknowledgments

This project was possible thanks to the support of the Texas Higher Education Coordinating Board, Advanced Technology Program under Grant 999903-165 (TEES 32190-71720ME). Acknowledgment is also given to D. Kontrovitz for making flow measurements in the test section.

References

[1]Chupp, R. E., Helms, H. E., McFadden, P. W., and Brown, T. R., "Evaluation of Internal Heat Transfer Coefficients for Impingement Cooled Turbine Blades," *Journal of Aircraft*, Vol. 6, No. 1, 1969, pp. 203–208; also AIAA Paper 68-564, Jan. 1968.

[2]Kercher, D. M., and Tabakoff, W., "Heat Transfer by a Square Array of Round Air Jets Impinging Perpendicular to a Flat Surface Including the Effect of Spent Air," *Journal of Engineering for Power*, Vol. 92, No. 1, 1970, pp. 73–82.

[3]Florschuetz, L. W., Truman, C. R., and Metzger, D. E., "Streamwise Flow and Heat Transfer Distribution for Jet Array Impingement with Crossflow," *Journal of Heat Transfer*, Vol. 103, No. 2, 1981, pp. 337–342.

[4]Florschuetz, L. W., Metzger, D. E., Su, C. C., Isoda, Y., and Tseng, H. H., "Heat Transfer Characteristics for Jet Array Impingement with Initial Crossflow," *Journal of Heat Transfer*, Vol. 106, No. 1, 1984, pp. 34–41.

[5]Behbahani, A. I., and Goldstein, R. J., "Local Heat Transfer to Staggered Arrays of Impinging Circular Air Jets," *Journal of Engineering for Power*, Vol. 105, No. 3, 1983, pp. 354–360.

[6]Downs, S. J., and James, E. H., "Jet Impingement Heat Transfer—A Literature Survey," American Society of Mechanical Engineers, ASME Paper 87-HT-35, 1987.

[7]Obot, N. T., and Trabold, T. A., "Impingement Heat Transfer Within Arrays of Circular Jets. Part I: Effects of Minimum, Intermediate, and Complete Crossflow for Small and Large Spacings," *Journal of Heat Transfer*, Vol. 109, No. 4, 1987, pp. 872–879.

[8]Viskanta, R., "Heat Transfer to Impinging Isothermal Gas and Flame Jets," *Experimental Thermal and Fluid Science*, Vol. 6, No. 1, 1993, 113–134.

[9]Huber, A. M., and Viskanta, R., "Effect of Jet-Jet Spacing on Convective Heat Transfer to Confined, Impinging Arrays of Axisymmetric Air Jets," *International Journal of Heat and Mass Transfer*, Vol. 37, No. 18, 1994, pp. 2859–2869.

[10]Huber, A. M., and Viskanta, R., "Comparison of Convective Heat Transfer to Perimeter and Center Jet in a Confined, Impinging Array of Axisymmetric Air Jets," *International Journal of Heat and Mass Transfer*, Vol. 37, No. 18, 1994, pp. 3025–3030.

[11]Bunker, R. S., and Metzger, D. E., "Local Heat Transfer in Internally Cooled Turbine Airfoil Leading Edge Regions: Part I—Impingement Cooling Without Film Coolant Extraction," *Journal of Turbomachinery*, Vol. 112, No. 3, 1990, pp. 451–458.

[12]Van Treuren, K. W., Wang, Z., Ireland, P. T., and Jones, T. V., "Detailed Measurements of Local Heat Transfer Coefficient and Adiabatic Wall Temperature Beneath an Array of Impingement Jets," *Journal of Turbomachinery*, Vol. 116, No. 3, 1994, pp. 369–374.

[13]Huang, Y., Ekkad, S. V., and Han, J. C., "Local Heat Transfer Coefficient Distribution Under an Array of Impinging Jets Using a Transient Liquid Crystal Technique," *Journal of Thermophysics and Heat Transfer*, Vol. 12, No. 1, 1998, pp. 73–79.

[14]Andrews, G. E., Bazdidi-Tehrani, F., Hussain, C. I., and Pearson, J. P., "Small Diameter Film Cooling Hole Heat Transfer: The Influence of the Hole Length," American Society of Mechanical Engineers, ASME Paper 91-GT-344, June 1991.

[15]Hollworth, B. R., and Dagan, L., "Array of Impinging Jets with Spent Fluid Removal Through Vent Holes on the Target Surface, Part I: Average Heat Transfer," *Journal of Engineering for Power*, Vol. 102, No. 4, 1980, pp. 994–999.

[16]Hollworth, B. R., Lehmann, G., and Rosiczkowski, J., "Arrays of Impinging Jets with Spent Fluid Removal Through Vent Holes on the Target Surface, Part II: Local Heat Transfer," *Journal of Engineering for Power*, Vol. 105, No. 4, 1983, pp. 393–402.

[17]Metzger, D. E., and Bunker, R. S., "Local Heat Transfer in Internally Cooled Turbine Airfoil Leading Edge Regions: Part II—Impingement Cooling with Film Coolant Extraction," *Journal of Turbomachinery*, Vol. 112, No. 3, 1990, pp. 459–466.

[18]Gillespie, D. R. H., Wang, Z., Ireland, P. T., and Kohler, S. T., "Full Surface Local Heat Transfer Coefficient Measurements in a Model of an Integrally Cast Impingement Cooling Geometry," *Journal of Turbomachinery*, Vol. 120, No. 1, 1998, pp. 92–99.

[19]Kline, S. J., and McClintock, F. A., "Describing Uncertainties in Single Sample Experiments," *Mechanical Engineering*, Vol. 75, No. 1, 1953, pp. 3–8.